ChemPubSoc Europe

DOI: 10.1002/cbic.201200733

VIP

Expansion of Access Tunnels and Active-Site Cavities Influence Activity of Haloalkane Dehalogenases in Organic Cosolvents

Veronika Stepankova,[a, b] Morteza Khabiri,[c, d] Jan Brezovsky,[a] Antonin Pavelka,[a] Jan Sykora,[e] Mariana Amaro,[e] Babak Minofar,[c] Zbynek Prokop,[a] Martin Hof,[e] Rudiger Ettrich,[c, d] Radka Chaloupkova,*[a] and Jiri Damborsky*[a, b]

The use of enzymes for biocatalysis can be significantly enhanced by using organic cosolvents in the reaction mixtures. Selection of the cosolvent type and concentration range for an enzymatic reaction is challenging and requires extensive empirical testing. An understanding of protein–solvent interaction could provide a theoretical framework for rationalising the selection process. Here, the behaviour of three model enzymes (haloalkane dehalogenases) was investigated in the presence of three representative organic cosolvents (acetone, formamide, and isopropanol). Steady-state kinetics assays, molecular dynamics simulations, and time-resolved fluorescence spectroscopy were used to elucidate the molecular mechanisms of enzyme–solvent interactions. Cosolvent molecules entered the enzymes' access tunnels and active sites, enlarged their volumes with no change in overall protein structure, but surprisingly did not act as competitive inhibitors. At low concentrations, the cosolvents either enhanced catalysis by lowering $K_{0.5}$ and increasing k_{cat}, or caused enzyme inactivation by promoting substrate inhibition and decreasing k_{cat}. The induced activation and inhibition of the enzymes correlated with expansion of the active-site pockets and their occupancy by cosolvent molecules. The study demonstrates that quantitative analysis of the proportions of the access tunnels and active-sites occupied by organic solvent molecules provides the valuable information for rational selection of appropriate protein–solvent pair and effective cosolvent concentration.

Introduction

The use of enzymes in organic solvents significantly expands their technological applications, by avoiding the limitations associated with aqueous solutions.[1–3] Organic solvents enhance the solubility of hydrophobic substrates, prevent undesirable water-induced side reactions, and even give rise to altered enzyme chemistries.[4–7] Enzyme-catalysed reactions that are not possible in aqueous solutions because of kinetic or thermodynamic constraints can become favourable in non-aqueous environments.[6] However, the presence of organic cosolvents in the reaction mixture can also lead to rapid enzyme inactivation by denaturation, conformational rigidity, or inhibition.[7–11] Several mechanistic studies of enzymatic catalysis in aqua-organic media have provided valuable information on the effects of cosolvents on enzyme function.[12–18] Still, our understanding of these effects is limited, and selection of an appropriate cosolvent type and concentration range for a particular enzymatic reaction poses a considerable challenge as it relies on extensive empirical testing.[19]

Hydrolases are widely used for biotransformations in organic solvents.[1] Haloalkane dehalogenases (HLDs, EC 3.8.1.5) are a good model for mechanistic studies, because of the wealth of information available about their structures, reaction mechanisms, and kinetics.[20–23] HLDs catalyse the hydrolytic cleavage of carbon–halogen bonds in a broad range of halogenated hydrocarbons, and structurally belong to the α/β-hydrolase superfamily.[24,25] The three-dimensional structure of a typical HLD is composed of two domains: a conserved α/β-hydrolase main domain, and a variable, helical cap domain.[26] The active site in an HLD is a hydrophobic pocket at the interface of the main and cap domains. The catalytic machinery comprises five resi-

[a] V. Stepankova, Dr. J. Brezovsky, A. Pavelka, Assoc. Prof. Z. Prokop, Dr. R. Chaloupkova, Prof. J. Damborsky
Loschmidt Laboratories, Department of Experimental Biology and Centre for Toxic Compounds in the Environment
Faculty of Science, Masaryk University
Kamenice 5A13, 625 00 Brno (Czech Republic)
E-mail: jiri@chemi.muni.cz
radka@chemi.muni.cz

[b] V. Stepankova, Prof. J. Damborsky
International Clinical Research Center
St. Anne's University Hospital
656 91 Brno (Czech Republic)

[c] Dr. M. Khabiri, Dr. B. Minofar, Assoc. Prof. R. Ettrich
Institute of Nanobiology and Structural Biology
Global Change Research Center, Academy of Sciences of the Czech Republic
373 33 Nove Hrady (Czech Republic)

[d] Dr. M. Khabiri, Assoc. Prof. R. Ettrich
Faculty of Sciences, University of South Bohemia
373 33 Nove Hrady (Czech Republic)

[e] Dr. J. Sykora, Dr. M. Amaro, Prof. M. Hof
J. Heyrovsky Institute of Physical Chemistry
Academy of Sciences of the Czech Republic
182 23 Praha (Czech Republic)

Supporting information for this article is available on the WWW under http://dx.doi.org/10.1002/cbic.201200733.

dues in the active-site pocket: a nucleophilic aspartate, a basic histidine, an aspartic or glutamic acid, and a tryptophan–tryptophan or tryptophan–asparagine pair. The active sites of HLDs differ in their size and accessibility to the solvent via the main and "slot" tunnels. The size, shape, physicochemical properties, and dynamics of the tunnels and active sites are key determinants of the activity and substrate specificity of HLDs.[27,28] The number of practical applications of HLDs, including biocatalysis, biodegradation, and biodetection, is increasing as knowledge of their properties and structure–function relationships improves.[29–31] However, the broader use of HLDs is limited by poor solubility of their substrates in water, thus necessitating the introduction of organic cosolvents into the reaction media. In a previous study, we investigated the catalytic properties of three HLDs (DbjA from *Bradyrhizobium japonicum* USDA110,[23] DhaA from *Rhodococcus rhodochrous* NCIMB13064,[32] and LinB from *Sphingobium japonicum* UT26)[27] in the presence of various concentrations of fourteen organic cosolvents.[33] The enzymes exhibited different levels of resistance towards the cosolvents tested, despite the fact that they all belong to the same protein family, share the topology of the catalytic residues, and catalyse hydrolytic dehalogenation by the same reaction mechanism.[20–23]

To better understand the molecular basis of these differences, we investigated the behaviour of DbjA, DhaA, and LinB in the presence of three representative organic cosolvents: acetone, formamide, and isopropanol. Molecular-dynamics simulations, time-resolved fluorescence spectroscopy, and steady-state kinetic measurements were employed to gain an insight into the mechanisms governing the enzyme–solvent interactions at the molecular level. In our study, four different mechanisms of enzyme activation and inhibition in the presence of organic cosolvents were identified. A broadly applicable computational method, involving molecular-dynamics simulations and quantitative analysis of cosolvent occupancies inside the access tunnels and active sites, was developed to aid the selection of an appropriate organic cosolvent. In this way, predicted changes in the accessibilities of the active site were confirmed by time-resolved and steady-state fluorescence spectroscopy.

Results

Kinetics of HLDs in organic cosolvents

To determine how organic cosolvents at non-denaturing concentrations affect the kinetic constants of HLDs, steady-state kinetic assays with isothermal titration calorimetry were conducted. The conversion of the substrate 1-iodohexane catalysed by DbjA, DhaA, or LinB in buffers containing formamide (5%, *v*/*v*), acetone (20%, *v*/*v*), or isopropanol (10%, *v*/*v*) was monitored at 25 °C, to allow non-denaturing conditions.[33] The kinetics data for DbjA and DhaA were analysed by using Equation (1), which describes cooperativity and substrate inhibition (Scheme 1 A , Figure S1 A and B in the Supporting Information); the data for LinB were fitted to Equation (2), which describes cooperativity and hyperbolic substrate inhibition (Scheme 1 B, Figure S1 C). The kinetics parameter values are presented in Table 1.

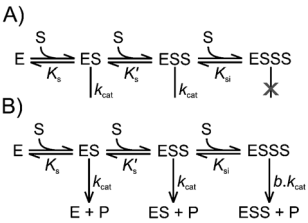

Scheme 1. Models showing A) cooperativity and substrate inhibition and B) cooperativity and hyperbolic substrate inhibition.

$$\frac{v}{V_{lim}} = \frac{[S]^n}{K_{0.5}^n + [S]^n(1 + [S]/K_{si})} \quad (1)$$

$$\frac{v}{V_{lim}} = \frac{[S]^n(1 + b[S]/K_{si})}{K_{0.5}^n + [S]^n(1 + [S]/K_{si})} \quad (2)$$

Here v is the enzyme's reaction velocity, V_{lim} is the maximum velocity, $K_{0.5}$ is the concentration of substrate at half maximum velocity, n is the Hill coefficient, [S] is the substrate concentration, K_{si} is the substrate inhibition constant, and b is a degree of partial inhibition. Interestingly, $K_{0.5}$ values for all three HLDs were generally lower in the presence of the tested organic cosolvents than in buffer alone, thus suggesting that organic cosolvents improve the affinity of the substrate for the free enzyme. The K_{si} values of all three catalysts were influenced differently by the organic cosolvents, thus indicating variation in changes in substrate inhibition of enzymes. Complete lack of substrate inhibition was observed only for LinB in the presence of acetone. The k_{cat} values were also affected by the addition of cosolvents: in general, increase in the catalytic constant (relative to buffer alone) was accompanied by enzyme activation, whereas a decrease in k_{cat} correlated with enzyme inhibition. In cases in which k_{cat} appeared to be unaffected by cosolvent (< 10% change), decreased enzyme activity was associated with a larger decrease in K_{si} than in $K_{0.5}$. Surprisingly, increased activity of LinB in the presence of isopropanol was observed, despite a larger decrease in K_{si} than in $K_{0.5}$ (compared to buffer alone), whereas k_{cat} was almost the same. This can probably be attributed to hyperbolic substrate inhibition with improved productivity of the triple-substrate-enzyme (ESSS) complex in the presence of isopropanol. We speculate that the ESSS complex might consist of two substrate molecules bound directly in the active-site cavity and a third molecule bound at the mouth of the access tunnel.

Molecular interactions of HLDs with organic cosolvents

Interactions between HLDs and the organic cosolvents formamide (5%, *v*/*v*), acetone (20%, *v*/*v*) and isopropanol (10%, *v*/*v*) were systematically studied by computer modelling. Molecular dynamics simulations showed the solvated structures of all the investigated enzymes were stable and equilibrated after 2 ns, with the average RMSD of Cα atoms reaching a plateau at less

Table 1. Steady-state kinetic parameters of DbjA, DhaA, and LinB determined for the conversion of 1-iodohexane in glycine buffer, with formamide (5%, *v/v*), acetone (20%, *v/v*) or isopropanol (10%, *v/v*).[a]

Enzyme	Reaction medium	k_{cat} [s^{-1}]	$K_{0.5}$ [μM]	K_{si} [mM]	n_H	*b*	a_r[b] [%]
DbjA	buffer	1.1	8.0	1.64	2.0	–[c]	100
	formamide	1.2	5.9	0.28	1.9	–[c]	82
	acetone	1.8	4.6	14.69	1.7	–[c]	123
	isopropanol	1.6	2.9	0.55	2.0	–[c]	118
DhaA	buffer	1.9	8.3	0.61	1.8	–[c]	100
	formamide	2.5	4.4	0.39	2.0	–[c]	130
	acetone	1.3	7.2	3.01	1.6	–[c]	93
	isopropanol	1.6	8.4	0.77	1.7	–[c]	99
LinB	buffer	5.2	29.5	0.08	1.5	0.25	100
	formamide	3.2	21.1	0.22	1.4	0.05	89
	acetone	2.4	6.7	–[c]	–[c]	–[c]	79
	isopropanol	5.0	19.2	0.02	1.4	0.50	117

k_{cat} catalytic constant; $K_{0.5}$ concentration of substrate at half maximal velocity; K_{si} substrate inhibition constant, n_H Hill coefficient; *b* degree of partial inhibition; a_r relative activity. [a] All measurements were performed at pH 8.6 and 25 °C. All parameters had standard errors of less than 10%. [b] The relative activities were expressed as a percentage of the specific activity in glycine buffer at substrate concentration of 0.2 mM. Specific activities (in μmol s^{-1} mg^{-1} of enzyme) of DbjA, DhaA and LinB in glycine buffer were 0.0110, 0.0135 and 0.0180, respectively. [c] Not detected.

than 1.7 Å from the initial structure (Table S2). The radii of gyration of HLDs in organic cosolvents, as well as their total solvent accessible surface areas, did not vary significantly from those of simulations in water (Table S2). The flexibility of all three proteins (expressed as total *B*-factors) was lower in almost all cosolvents than in water, except for LinB in acetone, for which a 30% higher value was observed. Although the effects of cosolvents on the overall structure of HLDs were minimal, the geometry and volumes of the active-site pockets (comprising access tunnels and the active sites) differed significantly between the simulations in water and with cosolvents (Figure 1 and Table S3).

The presence of cosolvents resulted in expansion of the access tunnel in DhaA by up to 200%, and isopropanol also caused an enlargement of the active site. Similarly, acetone and formamide caused expansion of the LinB tunnel by 200% and also a slight increase in the volume of the active site. In contrast, isopropanol caused a reduction (> 10%) of the LinB active site, whereas the access tunnel remained unaffected. For DbjA, only acetone had a significant effect on the structure of the active site and tunnel: decrease in volume of 20 and 30%, respectively.

Despite the different physicochemical properties of the cosolvent molecules and the anatomy of the enzyme active sites, all the cosolvents studied were able to penetrate into the access tunnels and active sites, thereby causing changes in hydration of these regions (Figure S2 and Table S4). By using newly developed algorithms, we determined the volume of the active site and entrance tunnel occupied by the organic solvent molecules (Figure 2 and Table S5). The occupancy of the access tunnels in LinB and DhaA by acetone was significantly higher than by formamide and isopropanol, whereas in DbjA all organic solvents occupied the access tunnel to a similar extent. However, for DbjA and formamide, the water molecules in the active site were nearly completely replaced by cosolvent mole-

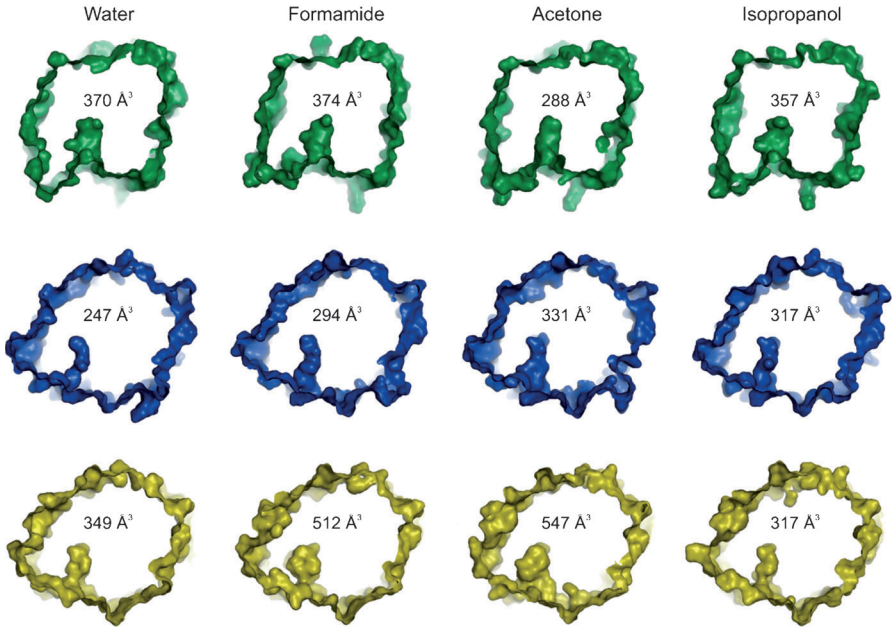

Figure 1. Representative geometries of DbjA (green), DhaA (blue), and LinB (yellow) active-site pockets (access tunnels and active sites) obtained from 35 ns molecular dynamics simulations in water or organic cosolvents. Only the protein surface and the active-site pockets are shown for clarity. The values given are the average volumes of the active-site pockets calculated over 4000 snapshots. See also Table S3 for average volumes of the active sites and the main tunnels.

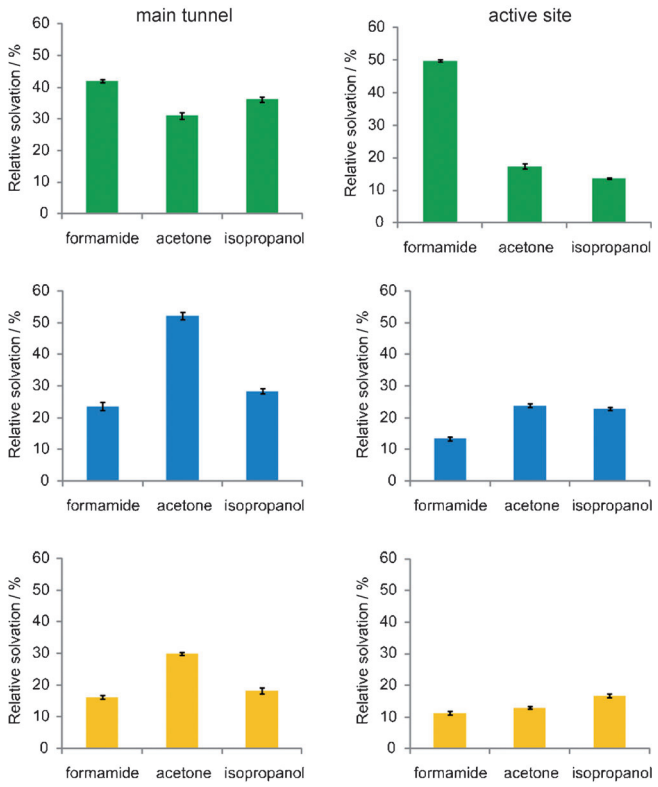

Figure 2. Relative solvation of DbjA (green), DhaA (blue), and LinB (yellow) is expressed as the ratio of the volume of the access tunnel or active site occupied by cosolvent molecules to the total volume of the access tunnel or active site. The algorithms used for calculation of occupancies are provided in the Supporting Information. See also Table S5 for average volumes of the active site and the main tunnels occupied by molecules of organic cosolvents.

cules, whereas in all other cases, the occupancy of the active site by organic solvent molecules was moderate.

Structural stability of HLDs in organic cosolvents

A combination of CD and fluorescence spectroscopy was used to reveal possible changes in the overall structures of DbjA, DhaA, and LinB in the presence of formamide (5%, *v/v*), acetone (20%, *v/v*), and isopropanol (10%, *v/v*) at 25 °C. The spectra were compared with those measured under native conditions (50 mM potassium phosphate buffer, pH 7.5) at 25 °C. This confirmed that addition of the selected organic cosolvents did not appreciably affect the overall conformation of any of the enzyme studied (Figure S3).

To address how the presence of cosolvent changes the regions relevant to enzyme function, coumarin dye was positioned at the tunnel mouth of the HLDs. This particular region is evolutionarily most variable and was suggested to be important in substrate recognition.[22] Acrylamide fluorescence quenching revealed that dye accessibility to the quencher molecules (K_{sv}) significantly increases in the presence of cosolvent in the order: acetone (20%, *v/v*) > formamide (5%, *v/v*) ≈ isopropanol (10%, *v/v*) > buffer (Table 2). This finding can be satisfactorily explained by broadening of the tunnel mouth. In

Table 2. Stern–Volmer constants and steady-state anisotropies of coumarin-labelled DhaA. Data were obtained for the coumarin located at the entrance of tunnel of DhaA leading to the active site, in glycine buffer, formamide (5%, *v/v*), acetone (20%, *v/v*), or isopropanol (10%, *v/v*).[a]

Reaction medium	K_{sv} [M^{-1}]	r_{st}
buffer	0.09	0.270
formamide	0.14	0.248
acetone	0.23	0.256
isopropanol	0.15	0.242

K_{SV}: Stern–Volmer constant; r_{st}: steady-state anisotropy. [a] All parameters had standard errors of less than 10%.

order to exclude enzyme denaturation and/or the possibility of dye release upon cosolvent addition, fluorescence steady-state anisotropies were recorded. Only a slight decrease (~10%) was observed for all investigated cosolvents (Table 2), thus indicating a small increase in the rotational diffusion of the dye–protein complex. To provide further molecular insight into the cosolvent effect, the time-dependent fluorescence shift (TDFS) was measured for acetone: this showed the highest accessibility to the quencher molecules (Table 2). As described earlier,[34,35] the overall magnitude of the TDFS reflects the level of hydration/polarity of the hydrated moieties in the probe vicinity, whereas TDFS kinetics reveals mobility. It is apparent from Table S6 that no significant changes were recorded for either the polarity parameter ($\Delta\nu$) or the mobility parameter (τ_R) in the presence of acetone (compared to buffer), within the time resolution of the experiment (30 ps). A difference was observed in the overall protein dynamics: only 70% of the TDFS was detected in the presence of acetone, whereas almost 90% of the TDFS was captured in buffer (Figure S4 and Table S6). A TDFS response on the timescale of several picoseconds has been demonstrated to be typical for neat solvent.[36,37] The observed acceleration of the solvent relaxation component indicates that the TDFS of coumarin at the tunnel mouth of DhaA sensed a considerably higher quantity of free solvent molecules in the presence of acetone than in pure buffer. This result confirms the hypothesis of tunnel expansion.

Discussion

The variability in enzyme efficiency in the presence of organic solvents can be generally attributed to changes in: 1) enzyme conformation and flexibility, 2) (de)solvation of the active site, 3) energetics of substrate desolvation, 4) steric hindrance restricting the accessibility of the substrate, and 5) competitive inhibition by the organic solvent molecules.[9–11] In a previous study, loss of HLD activity at high cosolvent concentrations was mainly attributed to alterations in enzyme secondary and tertiary structures, as detected by CD and fluorescence spectroscopy.[33] However, the spectroscopic data could not explain the observed enzyme activation and inhibition under non-denaturing cosolvent concentrations.

In this work, fluorescence quenching, time-dependent fluorescence shift, steady-state kinetics measurements, and molecular dynamics simulations were employed to gain a deeper un-

derstanding of the enzyme–solvent interactions at the molecular level. Formamide, acetone, and isopropanol were selected for this detailed analysis because of their different physicochemical properties and effects on the activity of the investigated enzymes, although a simple correlation between basic physicochemical properties and their effects could not be inferred. It was revealed that the organic solvent molecules affect the volume and geometry of the active-site pockets (i.e., access tunnels and active site cavities) to different extents. Both enlargement and constriction of the pockets were observed, without changes in overall protein structure. Solvent-induced widening of the substrate tunnel has been observed in cocrystallisation experimentation of heme monooxygenase P450 BM-3 with dimethyl sulfoxide.[38] The largest change in the pocket was observed for LinB, followed by DhaA. This could explain the complete denaturation of LinB and DhaA with increasing cosolvent concentration observed in our previous study.[33] In contrast, no enlargement of the pocket was detected for DbjA, which is possibly why DbjA exhibited the highest stability towards cosolvents.[33]

To understand the interactions of the organic solvent molecules with the functionally important regions of HLDs, we investigated their penetration into the access tunnels and active site cavities. All three organic solvents studied entered the access tunnels and the active site cavities within 35 ns in the molecular dynamics simulations. Although spontaneous exchange of cosolvent molecules between the active site and the surrounding environment was observed in some cases, the total number of organic solvent molecules in the active site remained almost constant. Penetration of polar organic solvent molecules into the tunnels and/or active sites was observed for *Candida antarctica* lipase B,[10,39] *Pseudomonas cepacia* lipase,[40] subtilisin BPN′,[41] subtilisin E,[7] subtilisin Carlsberg,[42] cytochrome P450 BM-3,[16,38] and pseudolysin[43] in molecular dynamics simulations and cocrystallisation experiments. One might expect involvement of competitive inhibition in cosolvent-induced inactivation of HLDs. However, the steady-state kinetics analysis revealed that the presence of organic solvent molecules inside the enzyme cavity increased substrate affinity for the free enzyme (decreased $K_{0.5}$) in most cases. Moreover, molecules of formamide and isopropanol appeared to improve the affinity of the substrate for the double-substrate–enzyme ESS complex (decreased K_{si}).

Two different mechanisms of cosolvent-induced inhibition were identified. Firstly, enzyme inactivation correlated with increased substrate inhibition (lower K_{si}), which was not sufficiently compensated for by an increase in substrate binding to the free enzyme (lower $K_{0.5}$). This behaviour is interesting, and to the best of our knowledge has not yet been described in the literature. Molecular dynamics simulations showed that this mechanism is associated with the most extensive occupancy of the active site by the organic solvent, accompanied by significant dehydration of the protein cavity. This mechanism was observed for DbjA in the presence of formamide, where the organic solvent filled about half of the DbjA active-site cavity, thereby resulting in an almost five-fold decrease in hydration. Secondly, diminishing enzyme activity was attributable to a reduction in the catalytic constant. For DhaA in acetone, organic solvent molecules predominantly occupied the access tunnel (connecting the active site cavity with the surrounding environment), thereby causing either substrate entry or product release to be impaired. For LinB in formamide and acetone, solvent molecules occupied only a small portion of the access tunnel, but resulted in its significant expansion.

Additionally, two mechanisms were identified for cosolvent-induced enzyme activation. Firstly, an increase in enzyme activity was attributed to an increase in the catalytic constant. The precise molecular basis for this effect is not known, but enhanced catalytic activity from improved stabilisation of the transition state has been previously reported.[44] Increased catalytic constants were observed for DbjA in acetone and isopropanol, and for DhaA in formamide. In the second mechanism, enzyme activation was caused by an increase in the degree of substrate inhibition partiality, thereby resulting in a higher productivity of the ESSS complex. Partial substrate inhibition was observed for LinB with 1-iodohexane but not for the other two enzymes; this might be explained by the size and spatial arrangement of the access tunnels.[23,27,32] LinB possesses the narrowest tunnel opening, which enable the formation of the productive ESSS complex. A higher productivity of the ESSS complex was observed in isopropanol. The molecular dynamics simulations suggested that molecules of isopropanol reduce the size of the LinB active-site pocket yet further, whereas formamide and acetone caused its expansion.

Conclusions

Water/organic cosolvent mixtures affect the physicochemical properties of all components in an enzymatic reaction mixture. The effect of organic cosolvent on enzyme structure and activity is complex and depends on the specific enzyme–substrate pair, cosolvent type, and cosolvent concentration. Four different molecular mechanisms were involved in these activation and inactivation events. The structural stability and catalytic activity of three representative HLDs in the presence of various concentrations of three organic cosolvents differed significantly. The inactivation of the enzymes at high cosolvent concentrations could be attributed to conformational changes in protein structure. At lower concentrations, both activation and inactivation took place, depending on: 1) the penetrability of the organic solvent molecules into the access tunnels and active-site cavities, and 2) expansion of access tunnels. The newly developed algorithms enabled calculation of the volumes of active-site pockets and their occupancy by the cosolvent molecules. These algorithms can be used to analyse trajectories from molecular dynamics simulations and to study the effect of water/organic cosolvent mixtures on enzyme catalytic performance. Our study contributes towards understanding protein–solvent interactions at the molecular level and paves the way for rational selection of appropriate protein–solvent pairs and effective cosolvent concentration.

Experimental Section

Organic solvents: Organic solvents were obtained from Sigma–Aldrich and were of the highest purity available. The cosolvents and their concentrations (formamide (5%, *v/v*), acetone (20%, *v/v*), and isopropanol (10%, *v/v*)) were selected based on their different physicochemical properties (Table S1) and substantially different effects on the activities of individual enzymes.[33]

Protein expression and purification: His-tagged DbjA from *Bradyrhizobium japonicum* USDA110,[23] DhaA from *Rhodococcus rhodochrous* NCIMB13064,[32] and LinB from *Sphingobium japonicum* (formerly *Sphingomonas paucimobilis*) UT26[27] were over-expressed in *Escherichia coli* BL21 cells by a previously described method.[21,45,46] Proteins were purified on a Ni-NTA Superflow Cartridges (Qiagen). His-tagged enzymes were bound to the resin in an equilibrating buffer (potassium phosphate buffer (20 mM, pH 7.5) containing sodium chloride (0.5 M) and imidazole (10 mM)), and unbound and weakly bound proteins were washed out. His-tagged enzymes were eluted in a buffer containing imidazole (300 mM). The active fractions were pooled and dialysed overnight against potassium phosphate buffer (50 mM, pH 7.5) and stored at 4 °C. Protein concentration was determined by the Bradford assay (Sigma–Aldrich). Purity was checked by SDS-PAGE.

Isothermal titration calorimetry: Substrate-to-product conversion by the enzymes was carried out by using a VP-ITC isothermal titration microcalorimeter (MicroCal/GE Healthcare) with the single-injection method. The substrate, 1-iodohexane, was dissolved to a concentration of approximately 0.3 mM in glycine buffer (100 mM, pH 8.6) containing an appropriate volume of organic cosolvent and equilibrated at 25 °C in the sample cell (1.4 mL). The reaction was initiated by injecting enzyme solution (10 μL, 1 mg mL^{-1}) dialysed overnight against the same solution as that used for dissolving the substrate. Heat flow (μcal s^{-1}) was recorded against time. The reaction rate was calculated according to Equation (3).

$$dQ/dt = -\Delta HV \cdot d[S]/dt \quad (3)$$

here V is the volume in the sample cell, [S] is substrate concentration, and ΔH is the enthalpy of the conversion of substrate to product. This was determined experimentally by titration of the substrate into the sample cell containing the enzyme. The evaluated rate of substrate depletion ($-d[S]/dt$), and corresponding substrate concentration were fitted by nonlinear regression to kinetic models by using Origin 6.1 software (OriginLab, Northampton, MA).

Molecular dynamics: Three-dimensional structures of the organic molecules were optimised and partial charges were calculated in Gaussian 03 by the Hartree–Fock method and the 6-31G* basic set.[47] Geometries were optimised at the MP2/6-31G* level. Topologies of all organic molecules were generated by using MKTOP[48] with the OPLSAA force field.[49–51] Three different mixtures of organic cosolvents with water (formamide (5%, *v/v*), acetone (20%, *v/v*) and isopropanol (10%, *v/v*)) were prepared to match the experimental conditions. Crystal structure coordinates for the haloalkane dehalogenases *Rhodococcus* sp. DhaA (PDB ID: 1CQW), *B. japonicum* DbjA (PDB ID: 3A2M), and *S. japonicum* LinB (PDB ID: 1MJ5) were downloaded from the Protein Data Bank, and substitutions V172A, I209L, and G292A were introduced into the structure of DhaA to match the primary structure of the enzyme from *Rhodococcus rhodochrous* NCIMB 13064.[32] Crystallographic water molecules were kept in place. Initially, crystal structures were energy minimised in vacuum by steepest-descent minimisation with at least 1000 steps. Minimised structures were solvated in pre-equilibrated water,[41] formamide (5%, *v/v*), acetone (20%, *v/v*) and isopropanol (10%, *v/v*) in a rectangular box, to a minimum distance of 15 Å from protein atoms. Sodium counter-ions were added by replacing water molecules to provide a neutral simulation box. All calculations were performed by using GROMACS 3.3.3[52,53] and extended OPLSAA force field.[50] The solvated systems were first energy minimised by using steepest descent, and the solvent was allowed to relax for 2 ns while keeping the protein restrained. Initial Maxwell–Boltzmann-weighted velocities were generated randomly, and the system was further equilibrated by gradually heating from 290 to 300 K over a 50 ps simulation. All simulations were run for 35 ns, with saving of coordinates every 5 ps; periodic boundary conditions and a 2 fs time step were employed. Weak temperature and pressure coupling with the coupling constants 0.1 ps[54] were used; the protein and solvent atoms had separate baths maintained at 300 K, and pressure maintained at 1 bar with a compressibility of 4.5×10^{-5} bar^{-1}. Electrostatic forces were evaluated by using the particle-mesh Ewald method[55] with a direct interaction cut-off of 10 Å. Van der Waals forces were evaluated with a Lennard–Jones potential of 10 Å cut-off. Covalent bond lengths were constrained by the linear constraint solver algorithm.[56]

Calculation of pocket volumes: A new computational procedure was developed to evaluate pocket volume. The procedure uses following information: a snapshot of the molecular dynamics simulation, atoms defining the location of the pocket of interest, and a sphere enclosing the measured space. Initially, pocket-defining atoms are used to locate the space of the pocket; a space accessible by a spherical probe is then determined; finally, the total volume of the accessible space is estimated and fractions of the volume occupied by the individual solvent molecules are determined (see the Supporting Information). The following settings were employed: the centre of a constraining sphere was placed at the CG atom of the catalytic nucleophile (LinB Asp108, DhaA Asp106, or DbjA Asp103), and the radius of the sphere was set to 8 Å and 11 Å for analysis of active-site cavity and whole catalytic pocket, respectively. The volume corresponding to the access tunnel was evaluated as the difference between the volume of the active-site cavity and the whole catalytic pocket. The probe radius for the pocket body calculation was 1.4 Å, and a grid resolution of 0.2 Å was employed for calculation of both the pocket body and the volumes. The probe was initially placed into a position that can accommodate a probe of radius 1.5-times larger than the desired probe radius (1.4 Å) within a maximum distance of 6 Å from the centre of the constraining sphere. Visual analysis of identified pockets was performed in VMD and PyMOL programs.[57,58]

Circular dichroism spectroscopy: CD spectra were performed at 25 °C by using a J-810 spectropolarimeter (Jasco) equipped with a Peltier thermostat (Jasco). Data were collected from 185 to 260 nm in buffer and from 200 to 260 in the presence of organic cosolvents, at 100 nm min^{-1}, with 1 s response time and 2 nm bandwidth. Spectra were recorded in a 0.1 cm quartz cuvette containing enzyme (0.25 mg mL^{-1}) in phosphate buffer (50 mM, pH 7.5) with defined amounts of organic cosolvent. Each spectrum is the average of 10 scans and baseline corrected. CD spectra were expressed as the mean residue ellipticity (θ_{MRE}) calculated according to Equation (4).

$$\theta_{MRE} = \theta_{obs} \cdot M_w \cdot 100/ncl \quad (4)$$

here θ_{obs} is the observed ellipticity in degrees, M_w is the protein molecular weight, n is number of residues, l is cell path length,

and c is the real protein concentration; the factor 100 originates from the conversion of the molecular weight to mg dmol^{-1}.

Fluorescence labelling: Engineered DhaA (50 μM) carrying the mutation H272F in the catalytic histidine was mixed with HaloTag coumarin ligand (Promega, catalogue no. G8581) at an enzyme/dye molar ratio of 3.3:1. The solution was incubated for 15 min at 37 °C to enable covalent attachment of the dye to the enzyme. The covalent binding was facilitated by HaloTag coumarin's containing a linker with a Cl atom at the end that serves as a substrate for enzyme DhaA H272F. Moreover, single-point mutation at position 272 prevented from the product release and the covalent complex Coumarin-DhaA was therefore preserved. Unbound probe was then removed by washing the enzyme immobilised on a HiTrap column (Amersham Biosciences/GE Healthcare) with phosphate buffer (100 mL, pH 7.5), and the eluted, labelled enzyme was dialysed with glycine buffer (pH 8.2). Cosolvent was then added to the sample. The proper incorporation of the dye into the enzyme was indicated by the linearity of the Stern–Volmer plots obtained by acrylamide quenching experiments.

Fluorescence steady-state spectroscopy: The fluorescence emission spectra, steady-state anisotropies, and quenching experiments were performed with a FluoroMax-4P spectrometer (HORIBA Jobin Yvon). For the intrinsic fluorophores tryptophan and tyrosine, fluorescence data were collected from 290 to 450 nm (excitation 280 nm, 50 nm min^{-1}, band-pass 1 nm). Spectra were recorded at 25 °C in a 0.5 cm quartz cuvette containing enzyme (0.25 mg mL^{-1}) in phosphate buffer (50 mM, pH 7.5) with a defined amount of organic cosolvent. Each spectrum was baseline corrected and expressed in terms of arbitrary units (instrument units of the fluorometer). In the case of DhaA labelled with coumarin, the fluorescence measurements were carried out in conditions as described for the intrinsic fluorophores with the following exceptions: samples were incubated at 10 °C, the steady-state emission spectra were excited at 373 nm and collected from 390 to 600 nm. When performing the fluorescence quenching measurements, samples were excited at 350 nm, and the emission was detected at 450 nm. The aliquots of acrylamide solution (4 M) were added directly to the protein sample in the cuvette with continuous stirring. The steady-state anisotropic values (r_{st}) were measured with polarisers inserted into the setup at the same wavelength regions as for the quenching experiments, and were calculated as described elsewhere.[59]

Fluorescence decay: Fluorescence decays were collected by using IBH 5000 U SPC equipment (HORIBA Jobin Yvon) with a picosecond diode laser (IBH NanoLED 11, 370 nm peak wavelength, 0.1 ns pulse width, 1 MHz repetition rate) and a cooled Hamamatsu R3809U-50 microchannel plate photomultiplier (Hamamatsu Photonics) with 30 ps resolution. Emission decays were recorded at a series of wavelengths spanning the steady-state emission spectrum (400–490 nm). Fluorescence decays were fitted to multiexponential functions, by using the iterative reconvolution procedure with IBH DAS6 software (HORIBA). To monitor TDFS, time-resolved emission spectra (TRES) were generated by the spectral reconstruction method and treated as described elsewhere.[59] In order to estimate to what extent TDFS kinetics is captured by the experiment, the emission spectrum at $t = 0$ was calculated independently.[59]

Acknowledgements

This research was supported by the Grant Agency of the Czech Republic (203/08/0114 and P503/12/0572), the Grant Agency of the Czech Academy of Sciences (IAA401630901) and the European Regional Development Fund (CZ.1.05/1.1.00/02.0123 and CZ.1.05/2.1.00/01.0001). MetaCentrum is acknowledged for providing access to computing facilities, supported by the Czech Ministry of Education of the Czech Republic (LM2010005). The National Centre for Bio-molecular Research is acknowledged for providing access to microcalorimeters. Brno City Municipality supported the work of A.P. with a Brno Ph.D. Talent Scholarship. M.H. acknowledges the Premium Academic Award from Academy of Science of the Czech Republic.

Keywords: enzyme catalysis · enzyme structure · haloalkane dehalogenases · molecular dynamics · organic cosolvents

[1] G. Carrea, S. Riva, *Angew. Chem.* **2000**, *112*, 2312 – 2341; *Angew. Chem. Int. Ed.* **2000**, *39*, 2226 – 2254.
[2] A. M. Klibanov, *Nature* **2001**, *409*, 241 – 246.
[3] R. K. Eppler, R. S. Komor, J. Huynh, J. S. Dordick, J. A. Reimer, D. S. Clark, *Proc. Natl. Acad. Sci. USA* **2006**, *103*, 5706 – 5710.
[4] A. Zaks, A. M. Klibanov, *Proc. Natl. Acad. Sci. USA* **1985**, *82*, 3192 – 3196.
[5] A. Zaks, A. Klibanov, *Science* **1984**, *224*, 1249 – 1251.
[6] C. H. Wong, *Science* **1989**, *244*, 1145 – 1152.
[7] S. Toba, K. M. Merz, Jr, *J. Am. Chem. Soc.* **1997**, *119*, 9939 – 9948.
[8] A. M. Klibanov, *Trends Biotechnol.* **1997**, *15*, 97 – 101.
[9] A. Schmid, J. S. Dordick, B. Hauer, A. Kiener, M. Wubbolts, B. Witholt, *Nature* **2001**, *409*, 258 – 268.
[10] M. Graber, R. Irague, E. Rosenfeld, S. Lamare, L. Franson, K. Hult, *Biochim. Biophys. Acta Proteins Proteomics* **2007**, *1774*, 1052 – 1057.
[11] A. L. Serdakowski, J. S. Dordick, *Trends Biotechnol.* **2008**, *26*, 48 – 54.
[12] L. M. Simon, M. Kotormán, G. Garab, I. Laczkó, *Biochem. Biophys. Res. Commun.* **2001**, *280*, 1367 – 1371.
[13] E. A. Belyaeva, D. V. Gra, N. L. Eremeev, *Biochemistry Mosc.* **2002**, *67*, 1032 – 1036.
[14] W. Tsuzuki, A. Ue, A. Nagao, *Biosci. Biotechnol. Biochem.* **2003**, *67*, 1660 – 1666.
[15] J. H. Yoon, D. Mckenzie, *Enzyme Microb. Technol.* **2005**, *36*, 439 – 446.
[16] D. Roccatano, T. S. Wong, U. Schwaneberg, M. Zacharias, *Biopolymers* **2006**, *83*, 467 – 476.
[17] C. B. Faulds, M. Pérez-Boada, A. T. Martínez, *Bioresour. Technol.* **2011**, *102*, 4962 – 4967.
[18] D. Roccatano, *Curr. Protein Pept. Sci.* **2008**, *9*, 407 – 426.
[19] E. Vazquez-Figueroa, V. Yeh, J. M. Broering, J. F. Chaparro-Riggers, A. S. Bommarius, *Protein Eng. Des. Sel.* **2008**, *21*, 673 – 680.
[20] D. B. Janssen, *Curr. Opin. Chem. Biol.* **2004**, *8*, 150 – 159.
[21] Y. Sato, M. Monincová, R. Chaloupková, Z. Prokop, Y. Ohtsubo, K. Minamisawa, M. Tsuda, J. Damborsky, Y. Nagata, *Appl. Environ. Microbiol.* **2005**, *71*, 4372 – 4379.
[22] E. Chovancová, J. Kosinski, J. M. Bujnicki, J. Damborský, *Proteins Struct. Funct. Bioinf.* **2007**, *67*, 305 – 316.
[23] Z. Prokop, Y. Sato, J. Brezovsky, T. Mozga, R. Chaloupkova, T. Koudelakova, P. Jerabek, V. Stepankova, R. Natsume, J. G. E. van Leeuwen, D. B. Janssen, J. Florian, Y. Nagata, T. Senda, J. Damborsky, *Angew. Chem.* **2010**, *122*, 6247 – 6251; *Angew. Chem. Int. Ed.* **2010**, *49*, 6111 – 6115.
[24] D. L. Ollis, E. Cheah, M. Cygler, B. Dijkstra, F. Frolow, S. M. Franken, M. Harel, S. J. Remington, I. Silman, J. Schrag, J. L. Sussman, K. H. G. Verschueren, A. Goldman, *Protein Eng.* **1992**, *5*, 197 – 211.
[25] M. Nardini, B. W. Dijkstra, *Curr. Opin. Struct. Biol.* **1999**, *9*, 732 – 737.
[26] K. H. Verschueren, J. Kingma, H. J. Rozeboom, K. H. Kalk, D. B. Janssen, B. W. Dijkstra, *Biochemistry* **1993**, *32*, 9031 – 9037.
[27] J. Marek, J. Vévodová, I. K. Smatanová, Y. Nagata, L. A. Svensson, J. Newman, M. Takagi, J. Damborský, *Biochemistry* **2000**, *39*, 14082 – 14086.
[28] M. Petrek, M. Otyepka, P. Banás, P. Kosinová, J. Koca, J. Damborský, *BMC Bioinf.* **2006**, *7*, 316.
[29] P. E. Swanson, *Curr. Opin. Biotechnol.* **1999**, *10*, 365 – 369.
[30] D. W. Campbell, C. Müller, K. F. Reardon, *Biotechnol. Lett.* **2006**, *28*, 883 – 887.
[31] Z. Prokop, F. Oplustil, J. DeFrank, J. Damborský, *Biotechnol. J.* **2006**, *1*, 1370 – 1380.

[32] J. Newman, T. S. Peat, R. Richard, L. Kan, P. E. Swanson, J. A. Affholter, I. H. Holmes, J. F. Schindler, C. J. Unkefer, T. C. Terwilliger, *Biochemistry* **1999**, *38*, 16105 – 16114.
[33] V. Stepankova, J. Damborsky, R. Chaloupkova, *Biotechnol. J.*; DOI: 10.1002/biot.201200378.
[34] L. Nilsson, B. Halle, *Proc. Natl. Acad. Sci. USA* **2005**, *102*, 13867 – 13872.
[35] P. Jurkiewicz, L. Cwiklik, P. Jungwirth, M. Hof, *Biochimie* **2012**, *94*, 26 – 32.
[36] M. L. Horng, J. A. Gardecki, A. Papazyan, M. Maroncelli, *J. Phys. Chem.* **1995**, *99*, 17311 – 17337.
[37] P. V. Kumar, M. Maroncelli, *J. Chem. Phys.* **1995**, *103*, 3038 – 3060.
[38] J. Kuper, T. S. Wong, D. Roccatano, M. Wilmanns, U. Schwaneberg, *J. Am. Chem. Soc.* **2007**, *129*, 5786 – 5787.
[39] P. Trodler, J. Pleiss, *BMC Struct. Biol.* **2008**, *8*, 9.
[40] Y. Liu, X. Zhang, H. Tan, Y. Yan, B. H. Hameed, *Process Biochem.* **2010**, *45*, 1176 – 1180.
[41] L. Yang, J. S. Dordick, S. Garde, *Biophys. J.* **2004**, *87*, 812 – 821.
[42] J. L. Schmitke, L. J. Stern, A. M. Klibanov, *Biochem. Biophys. Res. Commun.* **1998**, *248*, 273 – 277.
[43] D. Lousa, A. M. Baptista, C. M. Soares, *J. Chem. Inf. Model.* **2012**, *52*, 465 – 473.
[44] H. J. Wiggers, J. Cheleski, A. Zottis, G. Oliva, A. D. Andricopulo, C. A. Montanari, *Anal. Biochem.* **2007**, *370*, 107 – 114.
[45] Y. Nagata, K. Hynková, J. Damborský, M. Takagi, *Protein Expression Purif.* **1999**, *17*, 299 – 304.
[46] M. Pavlova, M. Klvana, Z. Prokop, R. Chaloupkova, P. Banas, M. Otyepka, R. C. Wade, M. Tsuda, Y. Nagata, J. Damborsky, *Nat. Chem. Biol.* **2009**, *5*, 727 – 733.
[47] *Gaussian 03*, M. J. Frisch, G. W. Trucks, H. B. Schlegel, G. E. Scuseria, M. A. Robb, J. R. Cheeseman, J. A. Montgomery, Jr., T. Vreven, K. N. Kudin, J. C. Burant, J. M. Millam, S. S. Iyengar, J. Tomasi, V. Barone, B. Mennucci, M. Cossi, G. Scalmani, N. Rega, G. A. Petersson, H. Nakatsuji, M. Hada, M. Ehara, K. Toyota, R. Fukuda, J. Hasegawa, M. Ishida, T. Nakajima, Y. Honda, O. Kitao, H. Nakai, M. Klene, X. Li, J. E. Knox, H. P. Hratchian, J. B. Cross, V. Bakken, C. Adamo, J. Jaramillo, R. Gomperts, R. E. Stratmann, O. Yazyev, A. J. Austin, R. Cammi, C. Pomelli, J. W. Ochterski, P. Y. Ayala, K. Morokuma, G. A. Voth, P. Salvador, J. J. Dannenberg, V. G. Zakrzewski, S. Dapprich, A. D. Daniels, M. C. Strain, O. Farkas, D. K. Malick, A. D. Rabuck, K. Raghavachari, J. B. Foresman, J. V. Ortiz, Q. Cui, A. G. Baboul, S. Clifford, J. Cioslowski, B. B. Stefanov, G. Liu, A. Liashenko, P. Piskorz, I. Komaromi, R. L. Martin, D. J. Fox, T. Keith, M. A. Al-Laham, C. Y. Peng, A. Nanayakkara, M. Challacombe, P. M. W. Gill, B. Johnson, W. Chen, M. W. Wong, C. Gonzalez, J. A. Pople, Gaussian, Inc., Wallingford, CT, **2004**.
[48] K. Kahn, T. C. Bruice, *J. Comput. Chem.* **2002**, *23*, 977 – 996.
[49] Y. P. Puhovski, B. M. Rode, *Chem. Phys.* **1995**, *190*, 61 – 82.
[50] W. L. Jorgensen, D. S. Maxwell, J. Tirado-Rives, *J. Am. Chem. Soc.* **1996**, *118*, 11225 – 11236.
[51] A. A. S. T. Ribeiro, B. A. C. Horta, R. B. de Alencastro, *J. Braz. Chem. Soc.* **2008**, *19*, 1433 – 1435.
[52] H. J. C. Berendsen, J. R. Grigera, T. P. Straatsma, *J. Phys. Chem.* **1987**, *91*, 6269 – 6271.
[53] H. J. C. Berendsen, D. van der Spoel, R. van Drunen, *Comp. Phys. Comm.* **1995**, *91*, 43 – 56.
[54] H. J. C. Berendsen, J. P. M. Postma, W. F. van Gunsteren, A. DiNola, J. R. Haak, *J. Chem. Phys.* **1984**, *81*, 3684.
[55] U. Essmann, L. Perera, M. L. Berkowitz, T. Darden, H. Lee, L. G. Pedersen, *J. Chem. Phys.* **1995**, *103*, 8577 – 8593.
[56] B. Hess, H. Bekker, H. J. C. Berendsen, J. G. E. M. Fraaije, *J. Comput. Chem.* **1997**, *18*, 1463 – 1472.
[57] W. L. Delano, *DeLano Scientific*, San Carlos, CA, USA, **2002**.
[58] W. Humphrey, A. Dalke, K. Schulten, *J. Mol. Graph.* **1996**, *14*, 33 – 38.
[59] A. Jesenská, J. Sýkora, A. Olžyn'ska, J. Brezovsky, Z. Zdrahal, J. Damborsky, M. Hof, *J. Am. Chem. Soc.* **2009**, *131*, 494 – 501.

Received: November 24, 2012
Published online on ■■ ■■, 0000

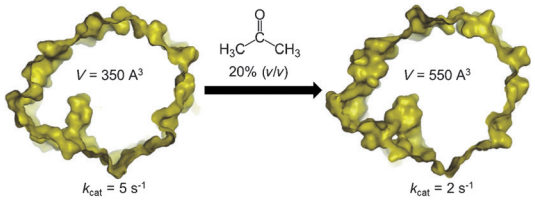

In the pocket: Newly developed algorithms enable calculation of the proportion of active-site pockets occupied by cosolvent molecules. These algorithms can be used to analyse trajectories from molecular dynamics simulations, and thus evaluate the effect of water/organic cosolvent mixtures on enzyme catalytic performance.

V. Stepankova, M. Khabiri, J. Brezovsky, A. Pavelka, J. Sykora, M. Amaro, B. Minofar, Z. Prokop, M. Hof, R. Ettrich, R. Chaloupkova, J. Damborsky**

■■ – ■■

VIP

Expansion of Access Tunnels and Active-Site Cavities Influence Activity of Haloalkane Dehalogenases in Organic Cosolvents